


Higher-Order Topological Insulator in Twisted Bilayer GrapheneMoon Jip Park,^{1,*} Youngkuk Kim^{2,†}, Gil Young Cho,^{3,‡} and SungBin Lee^{1,§}¹*Department of Physics, KAIST, Daejeon 34141, Republic of Korea*²*Department of Physics, Sungkyunkwan University, Suwon 16419, Republic of Korea*³*Department of Physics, Pohang University of Science and Technology (POSTECH), Pohang 37673, Republic of Korea* (Received 10 July 2019; published 22 November 2019)

Higher-order topological insulators are newly proposed topological phases of matter, whose bulk topology manifests as localized modes at two- or higher-dimensional lower boundaries. In this Letter, we propose the twisted bilayer graphenes with large angles as higher-order topological insulators, hosting topological corner charges. At large commensurate angles, the intervalley scattering opens up the bulk gap and the corner states occur at half filling. Based on both first-principles calculations and analytic analysis, we show the striking results that the emergence of the corner states do not depend on the choice of the specific angles as long as the underlying symmetries are intact. Our results show that the twisted bilayer graphene can serve as a robust candidate material of a two-dimensional higher-order topological insulator.

DOI: [10.1103/PhysRevLett.123.216803](https://doi.org/10.1103/PhysRevLett.123.216803)

Introduction.—Generalizing the concept of topology in diverse systems has been one of the most important topics in condensed matter physics [1,2]. One recently proposed interesting path of extending the knowledge of the topological phases of matter is to consider higher-order generalization [3,4]. That is to say, the band topology of d -dimensional insulator manifests as nontrivial $d-2$ or lower-dimensional boundary states, which is known as the higher-order topological insulator (HOTI) [5–36]. There have been several theoretical proposals of the higher-order topological insulators in both two- and three-dimensional solid state systems. For example, in three dimensions, the higher-order topological insulators harbor one-dimensional gapless modes, which is referred to as the hinge modes. Examples include a bismuth crystal [37], SnTe, surface-modified Bi₂TeI, BiSe, BiTe [8], phosphorene [18], van der Waals multilayers [30], and transition metal dichalcogenides $X\text{Te}_2$ [38]. In two dimensions, 0D localized modes appear at the corners of the two-dimensional materials, known as the corner states. The proposed examples are two-dimensional phosphorene [18], monolayer graphdiyne [39–41], bismuth [42], and continuum model of the twisted bilayer graphene [43,44].

Although there already exist a few candidate materials for the two-dimensional HOTIs, experimental signature that unambiguously identifies such phases remains elusive to date. To this end, it is desirable to identify higher-order topological materials that are readily available and highly controllable. Here, we propose that a large angle twisted bilayer graphene (TBG) is a generic higher-order topological insulator, characterized by the topologically protected corner states. TBG has clear advantages over other candidates for the experimental detection of the corner charge. (i) In our proposal, the HOTI is realized at half

filling; thus the corner state occurs without any fine-tuning of chemical potential, which is distinct from other cases [43,45]. (ii) In graphene, ultraclean transfer techniques are available that enables isolation from undesirable substrate effects [46]. (iii) The HOTI in graphene is a very unique system realized by intervalley scattering with negligible spin-orbit coupling. Thus, one can avoid any ambiguity arising from the spin-orbit coupling effect.

In this Letter, for the first time, we propose that the TBGs with large commensurate angles can be generically the higher-order topological insulators. We first present the first-principles calculations of the TBG at the commensurate angle, $\theta = 21.78^\circ$, as a representative example. In this case, we find that the sizable gap (~ 9 meV) exists which is originated from the absence of the $U(1)$ valley symmetry, $U(1)_v$. We then show that TBG has nontrivial higher-order band topology, characterized by the occurrence of topological corner states with the fractional electron charge $e/2$ in the mirror symmetric corners and C_6 symmetric corners. In addition, we generalize our discussion by showing that the nontrivial band topology is guaranteed to exist regardless of the specific commensurate twist angle or the microscopic details of the atomic structure as long as the underlying symmetries are preserved.

Lattice model and symmetries.—We begin our discussion by introducing the atomic structure and the associated crystalline symmetries of TBG. We consider a specific set of twisted bilayer structures that belong to the hexagonal space group no. 177 (point group D_6). The atomic configuration can be readily constructed by twisting AA-stacked bilayer graphene with respect to the collinear axis at the hexagonal center [see Figs. 1(a) and 1(b)]. The twist preserves both C_{6z} and C_{2x} about the out-of-plane z and in-plane x axes, respectively, which generate another

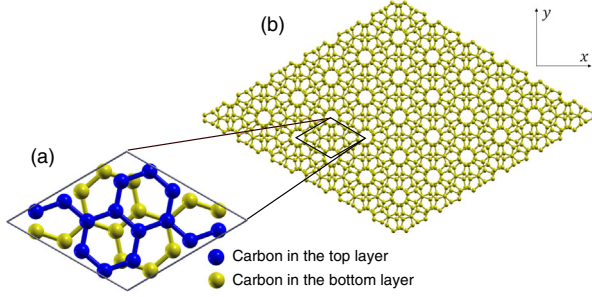


FIG. 1. Atomic configurations of the TBG in (a) a single moiré unit cell and (b) a finite-sized system with the twist angle, $\theta = 21.78^\circ$ ($p = 1, q = 3$).

important rotation C_{2y} about the y axis. The original translation symmetry is broken by the twist, but we can define the moiré translational symmetry, depending on the twist angle. For any coprime integers p and q , a twist by $\theta_{p,q} = \arccos[(3p^2 + 3pq + q^2/2)/(3p^2 + 3pq + q^2)]$ results in an enlarged moiré unit cell with the lattice constant $L = a\sqrt{(3p^2 + 3pq + q^2)/[\text{gcd}(q, 3)]}$ [47,48], where a is the original lattice constant and gcd represents the greatest common divisor.

Electronic energy bands.—In the limit where $\theta \lesssim 1^\circ$ without the lattice distortions, the moiré potential has long periodicity in real space, resulting in negligible interaction between valleys. In this limit, including the so-called *magic angles* where the Fermi velocity vanishes [49,50], each valley is decoupled and the $U(1)$ valley symmetry, $U(1)_v$, is approximately preserved and it, together with $C_{2z}\mathcal{T}$ symmetry, provides topological protection of four Dirac points associated with the \mathbb{Z}_2 -quantized Berry phases π [45,51,52]. Here, \mathcal{T} represents time-reversal symmetry, where $\mathcal{T}^2 = 1$ without spin-orbit coupling.

However, in the large angle limit $\theta \rightarrow 30^\circ$, which is the concern of this Letter, the $U(1)_v$ symmetry can be broken and the fourfold-degenerate Dirac points can split into two pairs of massive Dirac points, which here we claim to induce a HOTI phase. The intervalley coupling, and thus the gap opening between Dirac points, has a tendency to increase as the twist angle θ increases. Eventually, a sizable band gap of around 10 meV order opens at $\theta = 21.78^\circ$ ($p = 1, q = 3$) [53]. Focusing on this particular angle first, below we demonstrate the HOTI phase in TBG using first-principles calculations.

Figure 2(a) shows the density functional theory (DFT) electronic band structures of the TBG with $\theta = 21.78^\circ$. The results show that the band structure features a narrow gap of ~ 9 meV, which is more or less similar to the previous result of ~ 7 meV [53]. While a global direct band gap appears throughout the entire moiré Brillouin zone (BZ) between the conduction and valence bands, the minimum value occurs in the vicinity of K (as well as K') as shown in the right panel of Fig. 2(a). Using all the occupied 56 bands, we explore the higher-order band topology by directly

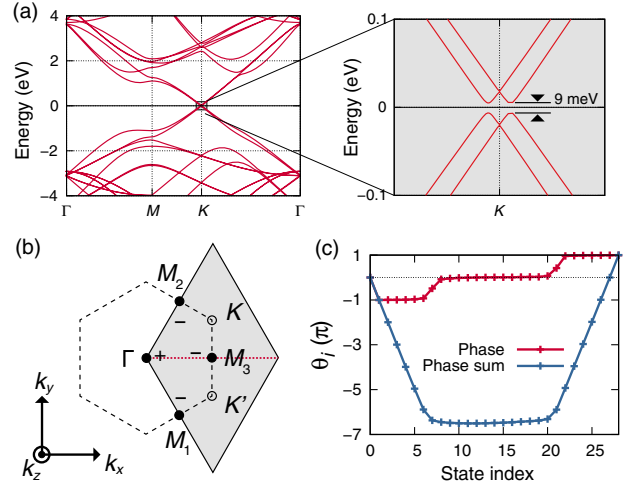


FIG. 2. (a) DFT band structures of TBG with $\theta = 21.78^\circ$. The right panel shows the magnified view of the region near K indicated by a gray box in the left panel. (b) Moiré Brillouin zone and the parity eigenvalues for half the occupied bands with negative parity. Time-reversal invariant momenta are indicated by a solid circle. A dotted red line highlights the high-symmetry C_{2x} -invariant line at $k_x = 0$. (c) Zak phase calculated using the mirror +1 bands along the mirror-invariant $k_x = 0$ line. The red curve represents the i th eigenphase θ_i . The blue curve represents the accumulated phase up to i th states, which results in π when summed up over all the occupied mirror+1 bands. The mirror winding number is calculated for the 56 occupied bands, comprising the same number of mirror+ and mirror− bands ($N_{\text{occ}}^+ = N_{\text{occ}}^- = 28$).

calculating a mirror-winding number and the second Stiefel-Whitney number.

Mirror-winding number.—Although we find that the Zak phase along any closed loop is trivial, a finer topological classification can be made along the mirror invariant line utilizing the presence of the mirror symmetry. The BZ has a mirror-invariant line Γ - M_3 - Γ preserving C_{2x} symmetry [see Fig. 2(b)]. Along this mirror invariant line, we can decompose the Hamiltonian into two distinct subsectors characterized by the mirror eigenvalues ± 1 . Then, one can define the \mathbb{Z}_2 mirror winding number [54–56] as the mirror-resolved Zak phase, ν_{\pm} , calculated along Γ - M_3 - Γ line for $C_{2x} = \pm 1$ subsector. The \mathbb{Z}_2 mirror winding number ν can be evaluated by

$$\nu = \nu_+ = \nu_- \pmod{2}, \quad (1)$$

where

$$\nu_{\pm} = \frac{1}{i\pi} \log \det[\mathcal{U}_{\pm}(\Gamma, M_3)\mathcal{U}_{\pm}(M_3, \Gamma)]. \quad (2)$$

Here, $\mathcal{U}_{\pm}(\mathbf{k}_1, \mathbf{k}_2) \equiv P \exp[i \int_{\mathbf{k}_1}^{\mathbf{k}_2} \mathcal{A}_{\pm}(\mathbf{k}) d\mathbf{k}] = \tilde{P}_{\pm}(\mathbf{k}_1) [\prod_k \tilde{P}_{\pm}(\mathbf{k})] \tilde{P}_{\pm}(\mathbf{k}_2)$, \mathcal{A}_{\pm} is the non-Abelian Berry connection evaluated from the \pm sector, respectively. P indicates the path ordering, and \tilde{P}_{\pm} is the projection operator to the

occupied mirror \pm subspace. Using all the occupied DFT bands, we calculate the eigenphase $\theta_{\pm,i} \equiv \text{Im} \log(u_{\pm,i})$, where $u_{\pm,i}$ is the i th eigenvalue of the Wilson loop matrix $\mathcal{U}_{\pm}(\Gamma, M_3)\mathcal{U}_{\pm}(M_3, \Gamma)$. The results, presented in Fig. 2(c), show that $\nu = \nu_{\pm} = +1$, confirming the nontrivial band topology.

Stiefel-Whitney number.—The physical manifestation of the nontrivial winding number $\nu = 1$ is the emergence of the topological corner states as we discuss later. Such corner states can be further established by the second Stiefel-Whitney number [57]. The TBG preserves the two-dimensional inversion symmetry C_{2z} , whose product with time-reversal symmetries $C_{2z}\mathcal{T}$ imposes that the Hamiltonian is real symmetric matrix, thus being characterized by the Stiefel-Whitney classes. While the first Stiefel-Whitney number ω_1 , which is equivalent to the Zak phase, is turned out to be trivial, the nontrivial second \mathbb{Z}_2 Stiefel-Whitney number ω_2 is expected from our DFT calculations. As proposed by Ahn *et al.* [57,58], we evaluate ω_2 from the parity eigenvalues of occupied bands at time-reversal invariant momenta (TRIM) $\Gamma_i \in \{\Gamma, M_1, M_2, M_3\}$ using

$$(-1)^{\omega_2} = \prod_{\Gamma_i \in \text{TRIM}} (-1)^{[N_{\text{occ}}^-(\Gamma_i)/2]}, \quad (3)$$

where $N_{\text{occ}}^-(\Gamma_i)$ is the number of occupied bands with an odd parity at Γ_i . Figure 2(c) shows the calculated parity eigenvalues at TRIM. We find that $\Gamma (M_{1,2,3})$ has 24 (30) odd bands out of the 56 occupied bands. Therefore the parities at $(\Gamma, M_1, M_2, M_3) = (+, -, -, -)$, leading to $\omega_2 = 1$.

The mirror winding number ν and the second Stiefel-Whitney number ω_2 are, in general, irrelevant topological invariants that depend on different symmetries (C_{2x} and $C_{2z}\mathcal{T}$, respectively). However, in the TBG, where both symmetries are present, we can formally equate these numbers. We decompose the Wilson loop into the two pieces of the Wilson lines related by the inversion symmetry [see Fig. 4(a)]. In this case, one can show the exact cancellation between the two Wilson lines up to the parity eigenvalues of C_{2z} as following,

$$\begin{aligned} & \det[\mathcal{U}_{\pm}(\Gamma, M_3)\mathcal{U}_{\pm}(M_3, \Gamma)] \\ &= \det\{\mathcal{U}_{\pm}(\Gamma, M_3)C_{2z}[C_{2z}^{-1}\mathcal{U}_{\pm}(M_3, \Gamma)C_{2z}]C_{2z}^{-1}\}, \\ &= \prod_{n \in \text{occ}, C_{2z} = \pm 1} \zeta_n(\Gamma)\zeta_n(M_3), \end{aligned} \quad (4)$$

where $\zeta_n(\mathbf{k})$ is the eigenvalue of C_{2z} at \mathbf{k} on n th band. Since C_{3z} guarantees the same parity structure of the bands at M_1, M_2 , and thus $\zeta_n(M_1)\zeta_n(M_2) = 1$ for any band index n . Therefore, we finally equate the mirror winding number $\nu = \nu_{\pm}$ to the second Stiefel-Whitney number ω_2 ,

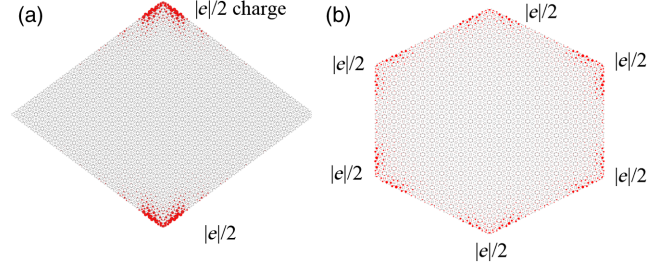


FIG. 3. The topological corner states derived from the tight binding model with (a) mirror symmetric and (b) C_6 symmetric open boundary conditions. The size of the red circles indicate the wave function amplitude. We find $(e/2)$ localized states on the corners in both boundary conditions.

$$\begin{aligned} (-1)^{\nu_{\pm}} &= \prod_{C_{2x}=1, n \in \text{occ}} \zeta_n(\Gamma)\zeta_n(M_3)\zeta_n(M_1)\zeta_n(M_2), \\ &= \prod_{\Gamma_i \in \text{TRIM}} (-1)^{N_{\text{occ}}^-(\Gamma_i)/2} \equiv (-1)^{\omega_2}. \end{aligned} \quad (5)$$

In the last line we used the absence of Zak phase (the first Stiefel-Whitney number $\omega_1 = 1$) along $\Gamma-M_3-\Gamma$, which enforces the same parity between the mirror-even and mirror-odd sectors [59].

Topological corner states.—After presenting the nontrivial topology of the bulk using the first-principles calculations, we utilize the tight-binding model [71] to demonstrate the topological corner states in a large sized TBG. We take the open boundary condition preserving the mirror symmetry. Figure 3(a) shows the tight-binding model calculations of the localized charge existing at the mirror symmetric corners. The mirror symmetry forces the corner charge to be equally distributed at each corner. As a result, they are fractionally quantized as $e/2$. In addition, one can also consider the boundary termination with C_6 symmetry. In such case, we can define \mathbb{Z}_6 valued C_6 quadrupole moment. This value is explicitly given as [72],

$$Q^{(6)} = \frac{e}{2}w_2 + \frac{e}{6}(\#C_3) \pmod{e}, \quad (6)$$

where $\#C_3$ counts the difference in the number of the occupied bands with \hat{C}_3 eigenvalue 1 between K and Γ . We find that the second term in Eq. (6) vanishes. Accordingly, $e/2$ localized corner charge occurs at each C_6 symmetric corners. Figure 3(b) shows such localized corner states derived from the tight binding model.

Generalization to an arbitrary twist angle.—It is important to note that the Stiefel-Whitney number, as well as the mirror winding number, is determined by the eigenstates at TRIM, whereas the low-energy physics of the TBG is described in the vicinity K and K' points in the moiré BZ. Therefore, the interlayer coupling does not alter the occupations of the TRIM points as compared to the noninteracting monolayer graphenes. As a consequence,

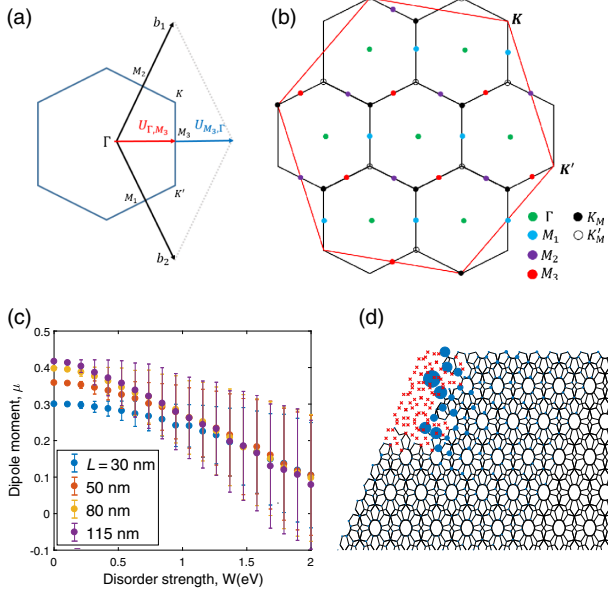


FIG. 4. (a) Schematic figure representing the Wilson loop along the mirror invariant line. We can decompose the Wilson loop into two lines related by the inversion symmetry (red and blue lines). (b) Figure of monolayer BZ and moiré BZ when $\theta = 21.78^\circ$. In the monolayer BZ, the TRIM points in the moiré BZ are always replicated odd times (in this case, seven times). (c) Averaged dipole moment of the corner state as a function of the disorder strength, W . We find that the dipole moment consistently survives up to 1 eV strength disorder regardless of the system size. (d) LDOS with the structural edge disorder. The corner state reconstruct its distribution and remained to be stable against the disorder (blue circle). Red cross indicates the removed sites.

the eigenvalues of C_{2z} and the Stiefel-Whitney number remains robust irrespective on the microscopic details of the interlayer coupling as long as the associated symmetries are preserved. Therefore, we can extend our analysis to arbitrary commensurate angles without the microscopic band structure calculations, assuming that all the low energy physics is described near K and K' points. Using this special property, we now show that the TBG in all other commensurate angles (arbitrary p , q) are higher-order topologically nontrivial at half filling. To do so, we first need to count the eigenvalues of inversion symmetry for the noninteracting monolayer graphene at the TRIM points in the moiré BZ. We first notice that $\{(3p^2 + 3pq + q^2)/[\text{gcd}(q, 3)]\} \equiv 2N + 1$ ($N \in \mathbb{Z}$) is always an odd integer and the area of the monolayer BZ fills $2N + 1$ numbers of the moiré BZ. For example, Fig. 4(b) shows that the monolayer BZ fills seven times that of a moiré BZ at $\theta = 21.78^\circ$. In generic commensurate angles, there exist $2N + 1$ occupied states at each TRIM point, say X , in the moiré BZ. In the original BZ of a monolayer, these states correspond to the occupied state of the monolayer graphene at distinct “non-TRIM” points related by the moiré reciprocal vectors [see Fig. 4(b)]:

$$X_{m,n} \equiv X + m\mathbf{b}_{M,1} + n\mathbf{b}_{M,2}, \quad (7)$$

where m , n are some integers. Among all the possible “independent” $2N + 1$ numbers of momentum points $X_{m,n}$, only $X_{0,0}$ is the inversion symmetric point in the monolayer BZ. Other $2N$ distinct momenta, $X_{m,n}$, are mapped to $X_{-m,-n}$ under inversion symmetry. Explicitly, one can choose a gauge such that \hat{C}_{2z} symmetry operator acts in the occupied eigenstates space as, $\hat{C}_{2z}|X_{m \neq 0, n \neq 0}\rangle = |X_{-m, -n}\rangle$. If we choose the basis of the occupied states at the TRIM points in the moiré BZ as $(|X_{0,0}\rangle, |X_{0,1}\rangle, |X_{-0,-1}\rangle, \dots, |X_{m,n}\rangle, |X_{-m,-n}\rangle)^T$, \hat{C}_{2z} operator in the moiré BZ is explicitly represented as,

$$\hat{C}_{2z} = \begin{pmatrix} \zeta(X) & 0 \\ 0 & \sigma_x \otimes I_N \end{pmatrix}, \quad (8)$$

where $\zeta(X)$ is the inversion eigenvalue of the occupied state at X in the monolayer graphene. Applying the eigenvalues of Eq. (8) to the second Stiefel-Whitney number in Eq. (3), the contributions from $X_{m \neq 0, n \neq 0}$ cancels out and we find that

$$(-1)^{\omega_2} = \zeta(M)\zeta(\Gamma). \quad (9)$$

In the monolayer graphene, the inversion eigenvalues at M point and Γ point always differ by the sign, so the second Stiefel-Whitney number must be always nontrivial, $\omega_2 = 1$. As a consequence, the TBG at all commensurate angles must be higher-order topologically nontrivial at half filling, as long as the gap is present at K point. In principle, the topological transition to the trivial state is possible if the additional gap closing occurs at M point. However, such gap closing contradicts with the previous first-principle calculations [73].

Effect of disorder.—In realistic graphene flakes, the disorder can break the underlying crystalline symmetries of the edge. To test the stability of the corner states against the disorder, we have simulated the tight-binding model in the presence of the Anderson disorder and the structural edge disorder [74] (see the Supplemental Material [59]). We calculate the dipole moment, μ , along the edge by computing the local density of states (LDOS). μ quantizes as $1/2$ if the corner is exactly localized at the corner, and vanishes if the edge is trivial. Figure 4(c) shows the dipole moment as a function of the Anderson disorder strength, W . We find that the dipole moment survives up to $W \approx 1$ eV, indicating that the corner states are robust against the finite disorder even in the absence of the crystalline symmetries. Beyond 1 eV scale, the bulk gap closes and the dipole moment becomes trivial. In the presence of the structural edge disorder, we also find the similar robustness against the disorder. In this case, the corner states reconstruct the spatial distribution and remained to be localized at the

corner [Fig. 4(d)], reflecting the robustness against the disorder [28,35,39].

Conclusion.—In summary, we have studied the higher-order topological properties of the TBG. When the twisted angle is large enough, the intervalley scattering plays an important role. Based on the first principle DFT calculation, we have demonstrated the existence of gap at charge neutrality due to the broken $U(1)_v$ symmetry. We have also shown that the TBG naturally hosts topological corner states that are protected by the mirror winding number. It is worth to note that the application of the pressure and strain can enhance the bulk gap. Yankowitz *et al.* [75] found that the application of the hydraulic pressure can drastically increase the bulk gap size. In addition, we have simulated the enhancement of the bulk gap as a function of the symmetry preserving strain [59]. The wide tunable band gap would allow more feasibility in the experimental realization of the HOTI.

It is worth emphasizing that the emergence of the HOTIs in TBG at any commensurate angles has generic properties induced by intervalley scattering and exists in any commensurate twist angles as long as the system opens a gap. In addition, the corner states occur at the half filling such that it does not require any fine-tuning of chemical potential. We also find that the corner states are robust against the finite disorder even in the absence of the crystalline symmetries. Our work provides important guidance for the search of the higher-order topological materials and paves the way for future experiments in the TBGs.

We appreciate Byungmin Kang, Seung-Hun Kang, Young-Woo Son, and Pilkyung Moon for fruitful discussion. M.J.P. and S.B.L. are supported by the KAIST startup, National Research Foundation Grant (No. NRF-2017R1A2B4008097) and BK21 plus program, KAIST. Y.K. was supported from NRF Grant (No. NRF-2019R1F1A1055205). The computational resource was provided from the Korea Institute of Science and Technology Information (KISTI).

*moonjippark@kaist.ac.kr

†youngkuk@skku.edu

‡gilyoungcho@postech.ac.kr

§sungbin@kaist.ac.kr

- [1] X.-L. Qi and S.-C. Zhang, *Rev. Mod. Phys.* **83**, 1057 (2011).
 [2] M. Z. Hasan and C. L. Kane, *Rev. Mod. Phys.* **82**, 3045 (2010).
 [3] W. A. Benalcazar, B. A. Bernevig, and T. L. Hughes, *Science* **357**, 61 (2017).
 [4] F. Zhang, C. L. Kane, and E. J. Mele, *Phys. Rev. Lett.* **110**, 046404 (2013).
 [5] W. A. Benalcazar, B. A. Bernevig, and T. L. Hughes, *Phys. Rev. B* **96**, 245115 (2017).
 [6] J. Langbehn, Y. Peng, L. Trifunovic, F. von Oppen, and P. W. Brouwer, *Phys. Rev. Lett.* **119**, 246401 (2017).

- [7] Z. Song, Z. Fang, and C. Fang, *Phys. Rev. Lett.* **119**, 246402 (2017).
 [8] F. Schindler, A. M. Cook, M. G. Vergniory, Z. Wang, S. S. P. Parkin, B. A. Bernevig, and T. Neupert, *Sci. Adv.* **4**, eaat0346 (2018).
 [9] M. Ezawa, *Phys. Rev. Lett.* **120**, 026801 (2018).
 [10] M. Serra-Garcia, V. Peri, R. Süsstrunk, O. R. Bilal, T. Larsen, L. G. Villanueva, and S. D. Huber, *Nature (London)* **555**, 342 (2018).
 [11] C. W. Peterson, W. A. Benalcazar, T. L. Hughes, and G. Bahl, *Nature (London)* **555**, 346 (2018).
 [12] S. Imhof, C. Berger, F. Bayer, J. Brehm, L. W. Molenkamp, T. Kiessling, F. Schindler, C. H. Lee, M. Greiter, T. Neupert, and R. Thomale, *Nat. Phys.* **14**, 925 (2018).
 [13] E. Khalaf, *Phys. Rev. B* **97**, 205136 (2018).
 [14] M. Geier, L. Trifunovic, M. Hoskam, and P. W. Brouwer, *Phys. Rev. B* **97**, 205135 (2018).
 [15] E. Khalaf, H. C. Po, A. Vishwanath, and H. Watanabe, *Phys. Rev. X* **8**, 031070 (2018).
 [16] F. K. Kunst, G. van Miert, and E. J. Bergholtz, *Phys. Rev. B* **97**, 241405(R) (2018).
 [17] Z. Yan, F. Song, and Z. Wang, *Phys. Rev. Lett.* **121**, 096803 (2018).
 [18] M. Ezawa, *Phys. Rev. B* **98**, 045125 (2018).
 [19] H. Xue, Y. Yang, F. Gao, Y. Chong, and B. Zhang, *Nat. Mater.* **18**, 108 (2019).
 [20] G. van Miert and C. Ortix, *Phys. Rev. B* **98**, 081110(R) (2018).
 [21] L. Trifunovic and P. W. Brouwer, *Phys. Rev. X* **9**, 011012 (2019).
 [22] M. Ezawa, *Phys. Rev. Lett.* **121**, 116801 (2018).
 [23] T. Goren, K. Plekhanov, F. Appas, and K. Le Hur, *Phys. Rev. B* **97**, 041106(R) (2018).
 [24] M. Lin and T. L. Hughes, *Phys. Rev. B* **98**, 241103(R) (2018).
 [25] T. Liu, Y.-R. Zhang, Q. Ai, Z. Gong, K. Kawabata, M. Ueda, and F. Nori, *Phys. Rev. Lett.* **122**, 076801 (2019).
 [26] M. Ezawa, *Phys. Rev. B* **98**, 201402(R) (2018).
 [27] M. Serra-Garcia, R. Süsstrunk, and S. D. Huber, *Phys. Rev. B* **99**, 020304(R) (2019).
 [28] H. Araki, T. Mizoguchi, and Y. Hatsugai, *Phys. Rev. B* **99**, 085406 (2019).
 [29] S. Franca, J. van den Brink, and I. C. Fulga, *Phys. Rev. B* **98**, 201114(R) (2018).
 [30] S. H. Kooi, G. van Miert, and C. Ortix, *Phys. Rev. B* **98**, 245102 (2018).
 [31] W. A. Wheeler, L. K. Wagner, and T. L. Hughes, *arXiv:1812.06990*.
 [32] B. Kang, K. Shiozaki, and G. Y. Cho, *arXiv:1812.06999*.
 [33] S. Ono, L. Trifunovic, and H. Watanabe, *arXiv:1902.07508*.
 [34] B. J. Wieder and B. A. Bernevig, *arXiv:1810.02373*.
 [35] A. Agarwala, V. Juricic, and B. Roy, *arXiv:1902.00507*.
 [36] D. Călugăru, V. Juričić, and B. Roy, *Phys. Rev. B* **99**, 041301(R) (2019).
 [37] F. Schindler, Z. Wang, M. G. Vergniory, A. M. Cook, A. Murani, S. Sengupta, A. Y. Kasumov, R. Deblock, S. Jeon, I. Drozdov, H. Bouchiat, S. Guéron, A. Yazdani, B. A. Bernevig, and T. Neupert, *Nat. Phys.* **14**, 918 (2018).
 [38] Z. Wang, B. J. Wieder, J. Li, B. Yan, and B. A. Bernevig, *Phys. Rev. Lett.* **123**, 186401 (2019).

- [39] B. Liu, G. Zhao, Z. Liu, and Z. F. Wang, *Nano Lett.* **19**, 6492 (2019).
- [40] E. Lee, R. Kim, J. Ahn, and B.-J. Yang, [arXiv:1904.11452](https://arxiv.org/abs/1904.11452).
- [41] X.-L. Sheng, C. Chen, H. Liu, Z. Chen, Y. Zhao, Z.-M. Yu, and S. A. Yang, [arXiv:1904.09985](https://arxiv.org/abs/1904.09985).
- [42] H. Kim, K. Jin, H. W. Yeom, B. Kang, and G. Y. Cho (to be published).
- [43] J. Ahn, S. Park, and B.-J. Yang, *Phys. Rev. X* **9**, 021013 (2019).
- [44] M. Kindermann, *Phys. Rev. Lett.* **114**, 226802 (2015).
- [45] Z. Song, Z. Wang, W. Shi, G. Li, C. Fang, and B. A. Bernevig, *Phys. Rev. Lett.* **123**, 036401 (2019).
- [46] H. C. Lee, W.-W. Liu, S.-P. Chai, A. R. Mohamed, A. Aziz, C.-S. Khe, N. M. Hidayah, and U. Hashim, *RSC Adv.* **7**, 15644 (2017).
- [47] L. Zou, H. C. Po, A. Vishwanath, and T. Senthil, *Phys. Rev. B* **98**, 085435 (2018).
- [48] J. M. B. Lopes dos Santos, N. M. R. Peres, and A. H. Castro Neto, *Phys. Rev. Lett.* **99**, 256802 (2007).
- [49] R. Bistritzer and A. H. MacDonald, *Proc. Natl. Acad. Sci. U.S.A.* **108**, 12233 (2011).
- [50] J. M. B. Lopes dos Santos, N. M. R. Peres, and A. H. Castro Neto, *Phys. Rev. B* **86**, 155449 (2012).
- [51] J. Ahn and B.-J. Yang, *Phys. Rev. Lett.* **118**, 156401 (2017).
- [52] C. Ma, Q. Wang, S. Mills, X. Chen, B. Deng, S. Yuan, C. Li, K. Watanabe, T. Taniguchi, D. Xu *et al.*, [arXiv:1903.07950](https://arxiv.org/abs/1903.07950).
- [53] S. Shallcross, S. Sharma, and O. A. Pankratov, *Phys. Rev. Lett.* **101**, 056803 (2008).
- [54] C.-K. Chiu, J. C. Y. Teo, A. P. Schnyder, and S. Ryu, *Rev. Mod. Phys.* **88**, 035005 (2016).
- [55] C.-K. Chiu, H. Yao, and S. Ryu, *Phys. Rev. B* **88**, 075142 (2013).
- [56] F. Zhang, C. L. Kane, and E. J. Mele, *Phys. Rev. Lett.* **111**, 056403 (2013).
- [57] J. Ahn, D. Kim, Y. Kim, and B.-J. Yang, *Phys. Rev. Lett.* **121**, 106403 (2018).
- [58] J. Ahn, S. Park, D. Kim, Y. Kim, and B.-J. Yang, [arXiv:1904.00336](https://arxiv.org/abs/1904.00336).
- [59] See Supplemental Material at <http://link.aps.org/supplemental/10.1103/PhysRevLett.123.216803> for detailed calculations, which includes Ref. [60–70].
- [60] P. Giannozzi *et al.*, *J. Phys. Condens. Matter* **21**, 395502 (2009).
- [61] J. P. Perdew and A. Zunger, *Phys. Rev. B* **23**, 5048 (1981).
- [62] A. M. Rappe, K. M. Rabe, E. Kaxiras, and J. D. Joannopoulos, *Phys. Rev. B* **41**, 1227 (1990).
- [63] N. J. Ramer and A. M. Rappe, *Phys. Rev. B* **59**, 12471 (1999).
- [64] H. J. Monkhorst and J. D. Pack, *Phys. Rev. B* **13**, 5188 (1976).
- [65] S. Grimme, *J. Comput. Chem.* **27**, 1787 (2006).
- [66] A. Kerelsky, L. J. McGilly, D. M. Kennes, L. Xian, M. Yankowitz, S. Chen, K. Watanabe, T. Taniguchi, J. Hone, C. Dean, A. Rubio, and A. N. Pasupathy, *Nature (London)* **572**, 95 (2019).
- [67] M. L. Sancho, J. L. Sancho, and J. Rubio, *J. Phys. F* **14**, 1205 (1984).
- [68] M. R. Hirsbrunner, T. M. Philip, B. Basa, Y. Kim, M. J. Park, and M. J. Gilbert, *Rep. Prog. Phys.* **82**, 046001 (2019).
- [69] M. Evaldsson, I. V. Zozoulenko, H. Xu, and T. Heinzel, *Phys. Rev. B* **78**, 161407(R) (2008).
- [70] E. R. Mucciolo, A. H. Castro Neto, and C. H. Lewenkopf, *Phys. Rev. B* **79**, 075407 (2009).
- [71] P. Moon and M. Koshino, *Phys. Rev. B* **87**, 205404 (2013).
- [72] W. A. Benalcazar, T. Li, and T. L. Hughes, *Phys. Rev. B* **99**, 245151 (2019).
- [73] S. Shallcross, S. Sharma, E. Kandelaki, and O. A. Pankratov, *Phys. Rev. B* **81**, 165105 (2010).
- [74] J. Li, I. Martin, M. Büttiker, and A. F. Morpurgo, *Nat. Phys.* **7**, 38 (2011).
- [75] M. Yankowitz, J. Jung, E. Laksono, N. Leconte, B. L. Chittari, K. Watanabe, T. Taniguchi, S. Adam, D. Graf, and C. R. Dean, *Nature (London)* **557**, 404 (2018).